Parametric resonance for vibration energy harvesting with design techniques to passively reduce the initiation threshold amplitude

Yu Jia, Jize Yan, Kenichi Soga and Ashwin A Seshia

Department of Engineering, University of Cambridge, Trumpington Street, Cambridge CB2 1PZ, UK

E-mail: yj252@cam.ac.uk, jy242@cam.ac.uk, ks207@cam.ac.uk, aas41@cam.ac.uk

Abstract.

A vibration energy harvester designed to access parametric resonance can potentially outperform the conventional direct resonant approach in terms of power output achievable given the same drive acceleration. Although linear damping does not limit the resonant growth of parametric resonance, a damping dependent initiation threshold amplitude exists and limits its onset. Design approaches have been explored in this paper to passively overcome this limitation in order to practically realise and exploit the potential advantages. Two distinct design routes have been explored, namely an intrinsically lower threshold through a pendulum-lever configuration and amplification of base excitation fed into the parametric resonator through a cantilever-initial-spring configuration. Experimental results of the parametric resonant harvesters with these additional enabling designs demonstrated up to an order of magnitude lower initiation threshold than otherwise, while attaining a much higher power peak than direct resonance.

PACS numbers: 07.07.Mp, 89.30.-g, 07.07.Df

Keywords: parametric, resonance, vibration, energy harvesting, initiation, threshold

Submitted to: *Smart Mater. Struct.*

1. Introduction

The fundamental mode of direct mechanical resonance has served as the basis for the conventional resonant-based vibration energy harvesting [1]. However, it is neither the sole nor the best resonant phenomenon that can be exploited for mechanical amplification to maximise mechanical-to-electrical energy conversion for vibration energy harvesting. This paper explores an alternative candidate: parametric resonance, which instead of exhibiting a forced response, involves a time dependent modulation in at least one of the homogenous system parameters at specific frequency and amplitude conditions. Once activated, unlike its direct resonant counterpart,

the oscillatory amplitude growth of parametric resonance does not saturate due to linear damping and only settles with the rise of vibrational nonlinearities at high amplitudes [2, 3]. The wider transducer community has dubbed this as the 'parametric amplification effect' employed to achieve higher input-to-output sensitivity than direct resonance [4, 5, 6, 7].

A critical onset condition is a damping-dependent initiation threshold amplitude, which must be fulfilled prior to accessing this alternative resonant regime, otherwise the steady state oscillatory response returns to zero. This initiation threshold, as well as the operational frequency bandwidth of the parametric resonant peaks, rapidly recede with increasing damping [2, 8]. This results in the elusiveness of parametric resonance despite its theoretical existence in almost all systems [9]. Previous studies by the authors have demonstrated over an order of magnitude higher power output when the same system is driven into parametric resonance rather than direct resonance for both macro-scale [10, 11] and MEMS-scale devices [12, 13, 14], while demonstrating the parametric resonant effect for all of the major transducers: electromagnetic [10], piezoelectric [11] and electrostatic [13]. This study investigates various design routes to overcome the threshold limitation and realise parametric resonance at practical vibrational acceleration levels (assumed to be $\sim$1's ms^{-2}).

2. Background

Any vibratory system can theoretically exhibit both direct resonance and parametric resonance depending on the nature of the excitation and boundary conditions. They can be respectively represented by equations 1 and 2.

$$\ddot{x} + c\dot{x} + \omega_0^2 x = F\cos(\omega t) \tag{1}$$

$$\ddot{x} + c\dot{x} + (\omega_0^2 + 2\varepsilon\cos(\omega t))x = 0 \tag{2}$$

where, x is the oscillatory displacement in the x plane, c is the damping, ω_0 is the natural frequency, ω is the drive frequency, F is the direct forcing amplitude in the x plane, ε is the parametric excitation amplitude typically orthogonal to the x plane and t is the time domain; also, unit mass are assumed in these particular equations.

Equation 1 can represent a generic second order mass-spring-damper system where a forced periodic excitation matching the natural frequency yields the fundamental mode of direct resonance ($\omega = \omega_0$). Even when the excitation frequency operates outside the resonant bandwidth, a forced response can be observed, albeit relatively minuscule.

On the other hand, parametric resonance represented by a form of the damped Mathieu equation in equation 2, does not rely on forced excitation but rather a periodic variation in one of its homogenous system parameters. Parametric excitation is typically orthogonal (but not exclusively) to the plane of the oscillatory displacement. Equation 2 can be further reduced to the classical damped Mathieu equation shown equation 3 [8].

$$\ddot{x} + c\dot{x} + (\delta + 2\varepsilon\cos(2t))x = 0 \tag{3}$$

where, δ is the natural frequency squared and $\omega = 2$. Figure 1 is known as the Strutt diagram [2] and is the stability chart for δ and ε parameters in equation 3. The unshaded area is the stable region where oscillatory displacement x has bounded solutions and converges to zero at steady state. The shaded unstable region is where

the onset of parametric resonance can be observed and the oscillatory amplitude builds up with time until a shift in eigenfrequency from nonlinearities saturates the resonant growth.

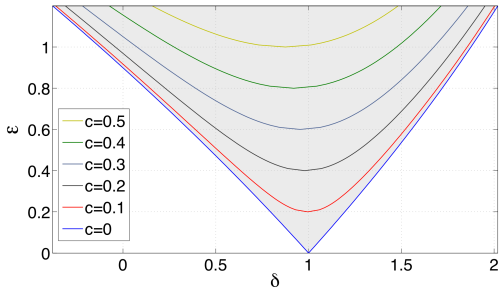

Figure 1: Strutt diagram for principal (1st order) parametric resonance. Shaded area represent the instability region where parametric resonance can be achieved, which elevates away from the horizontal base axis with increasing damping, thus creating an initiation threshold amplitude that excitation amplitude must attain.

Parametric resonance can be activated when the excitation frequency ω is in the vicinity of $2\omega_0/\mathrm{n}$, where ω_0 is the natural frequency and n is a positive integer representing the order number of the parametric resonance. Therefore, the principal (1st order) parametric resonance can be accessed when the excitation frequency is $2\omega_0$, which corresponds to $\delta = 1$ in figure 1. The second order can then be observed at $\delta = 4$, the third order at $\delta = 9$, so on and so forth.

The response frequency for any order of parametric resonance is around the natural frequency. As damping c increases, the unstable region elevates away from the horizontal axis in the Strutt diagram and an initiation amplitude threshold manifests, which the excitation amplitude need to minimally attain prior to accessing parametric resonance even if the desired frequency is matched.

The initiation threshold amplitude has been previously shown to be a key limiting factor in accessing the profitable regions of parametric resonance within practical acceleration levels and damping conditions [15, 7]. This is especially true for energy harvesting as the technology relies on electrical damping to extract energy. Active actuators have been used in sensor applications to realise the parametric amplification effect [16, 17], however, extra power expenditure is counterintuitive for energy harvesting. In the meantime, the acceleration levels of real world infrastructural vibrations are typically small (0.1's ms^{-2} to 1's ms^{-2}).

Design techniques illustrated in figure 2 have been previously proposed by the authors [12] to passively minimise this critical threshold in order to practically realise the profitable regions of the parametric resonance at lower acceleration levels. This paper presents the detailed experimental investigation of design iterations stemming from both of the proposed design routes.

Route I represents an electrically undamped parametric resonator coupled to a subsidiary mechanical amplifier where electrical damping is applied. The instability region in Route I is intrinsically lowered towards the horizontal axis in figure 1. Route II employs an electrically undamped mechanical amplifier as an initial spring to magnify the base excitation fed into the electrically damped parametric resonator. Here, the horizontal axis in figure 1 is brought up towards the instability region.

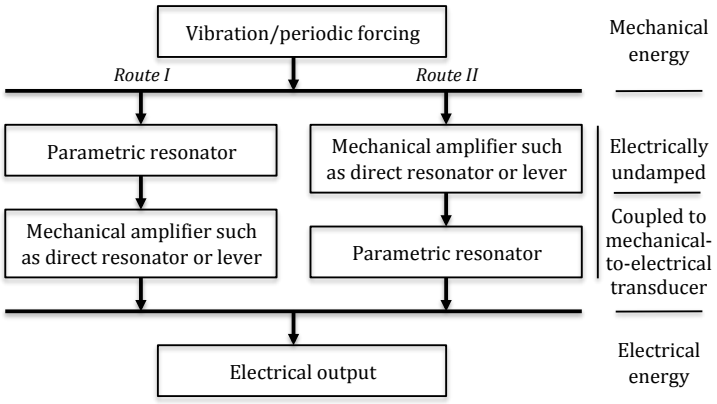

Figure 2: Design routes to minimise the initiation threshold amplitude to activate parametric resonance at lower acceleration levels..

3. Route I: electromagnetic pendulum and lever configuration

3.1. Design

Figure 3 presents a design iteration of Route I described in figure 2. Figure 3a is a simple pendulum where the oscillatory angular displacement is directly damped by an electromagnetic transducer. Figure 3b consists of an electrically undamped pendulum on the left-hand-side of the pivot, which is allowed to freely experience a build up of the oscillatory angular displacement with minimal effect from the electrical damping of the transducer. As the pendulum oscillates, the periodic unbalancing of the lever beam oscillates the right-hand-side of the lever beam in the x plane, which is electrically damped by an electromagnetic transducer.

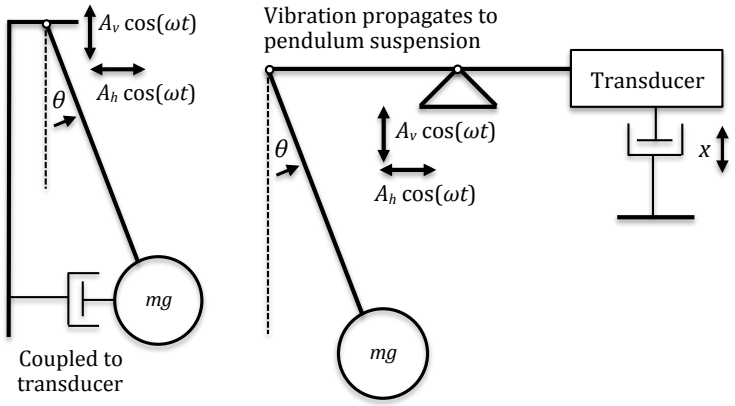

(a) Pendulum

(b) Pendulum coupled to a lever

Figure 3: Design iteration of a parametric resonator (pendulum) with intrinsically low initiation threshold by electrically damping the displacement x of the other end of the lever beam instead of the pendulum displacement θ.

Horizontal excitation of the pendulum corresponds to direct excitation as given

in equation 4.

$$\ddot{\theta} + c\dot{\theta} + \omega_0^2 \sin\theta - \omega_h^2 \frac{A_h}{l} \cos(\omega_h t) = 0 \tag{4}$$

where, θ is the angular displacement, ω_h is the excitation frequency in the horizontal axis, A_h is the excitation displacement amplitude in the horizontal axis and l is the pendulum length. Equation 5 governs the parametric excitation in the vertical axis.

$$\ddot{\theta} + c\dot{\theta} + (\omega_0^2 + \omega_v^2 \frac{A_v}{l} \cos(\omega_v t)) \sin\theta = 0 \tag{5}$$

where, ω_v is the excitation frequency in the vertical axis and A_v is the excitation displacement amplitude in the vertical axis. The combination of horizontal (direct) and vertical (parametric) excitations are governed by equation 6.

$$\ddot{\theta} + c\dot{\theta} + (\omega_0^2 + \omega_v^2 \frac{A_v}{l} \cos(\omega_v t)) \sin\theta - \omega_h^2 \frac{A_h}{l} \cos(\omega_h t) = 0 \tag{6}$$

Detailed governing equations and numerical analysis of this pendulum-lever system, along with the electromagnetic transduction, have been explored in a previous macro-scale investigation [10].

SolidWorks schematics of the prototypes explored here, based on the basic working mechanisms illustrated in figures 3a and 3b, are shown in figures 4 and 5 respectively.

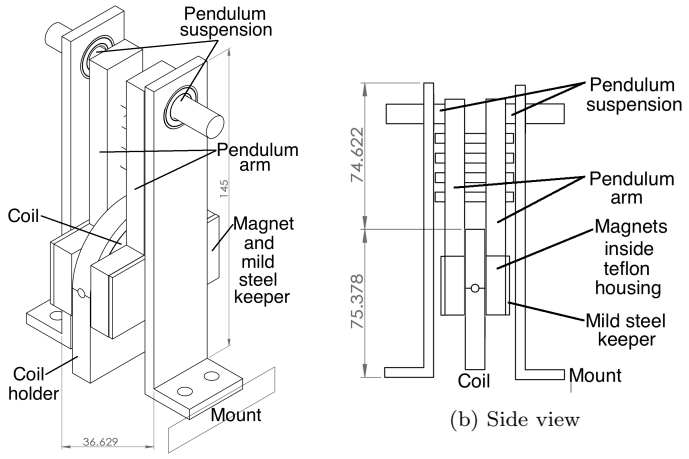

(a) Dimetric view

(b) Side view

Figure 4: SolidWorks drawings of the sole pendulum prototype, dubbed Swing.

Both prototypes employ electromagnetic transducers to convert mechanical energy into electrical energy. The first prototype (figure 4) is essentially a sole pendulum with magnets as its pendulum mass, moving against a fixed coil. The second prototype (figure 5) consists of an eccentric pendulum on one side of the lever beam while a counter mass made up of magnets rests on the other side of the lever beam. A coil is fixed against these magnets to complete the transducer.

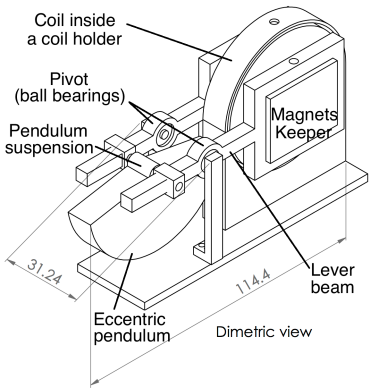

(a) Dimetric view

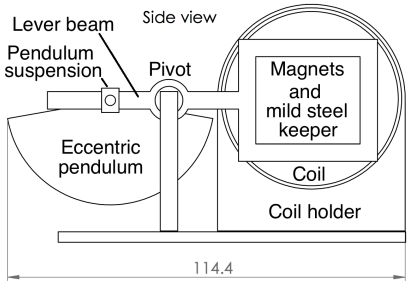

(b) Side view

Figure 5: SolidWorks drawings of the pendulum-lever prototype, dubbed Corsair.

3.2. Apparatus

The experimental prototypes shown in figures 6 (dubbed Swing) and 7 (dubbed Corsair) are iterations of the designs from figures 3a and 3b respectively and the realisation of the schematics shown in figures 4 and 5 respectively. Both prototypes are approximately 300 cm^3 in practical device volume at rest, while Corsair has $\sim$80 cm^3 and Swing has $\sim$150 cm^3 in component volume. The harvesters were mounted on a shaking table, which was driven by an air-cooled electromechanical shaker controlled by an external function generator and an accelerometer was attached to the shaking platform to quantify the applied driving force.

The electromagnetic transducers of both harvesters employ orthocyclically wound copper coils with 50 mm outer diameter, 5 mm inner diameter, 10 mm depth, 90 μ wire diameter. The magnets were sintered neodymium iron boron (NdFeB). Corsair contains four rectangular magnets (grade N35H) with individual dimensions of 30 mm length, 10 mm width and 5 mm depth. Swing consists of four circular magnets (grade N38H) with individual dimensions of 10 mm diameter and 10 mm depth. The four-magnet configuration [18] is employed to maximise flux density through the coil. The coil is positioned in a sandwich configuration in between each pair of magnets with an approximately 1 mm air gap between the magnet and the coil on either side. Additionally, two pieces of 1 mm thick rectangular mild steel plates have been magnetically attached to the sides of the magnets facing away from the coil to act as the magnetic flux keeper to further concentrate the flux density within the transducer.

Optimal electrical load was experimentally found to be between 15 kΩ and 20 kΩ for both devices through impedance matching and the coils measure electrical resistance of 15 ± 1 kΩ. Although the experimentally matched optimal load resistance varies depending on amplitude and the specific resonant regime, the variation is negligible for the studied amplitude and frequency ranges. Lubricated ball bearings have been used for minimal mechanical damping and energy loss from the cyclic motions of the pendulum suspension in the Swing and the pivot of the lever beam for the Corsair. The magnets constituent the primary mass of the pendulum of the Swing. The electromagnetic transducer is directly coupled to this pendulum mass. The Corsair on the other hand, utilises an eccentric pendulum mass to conserve volume

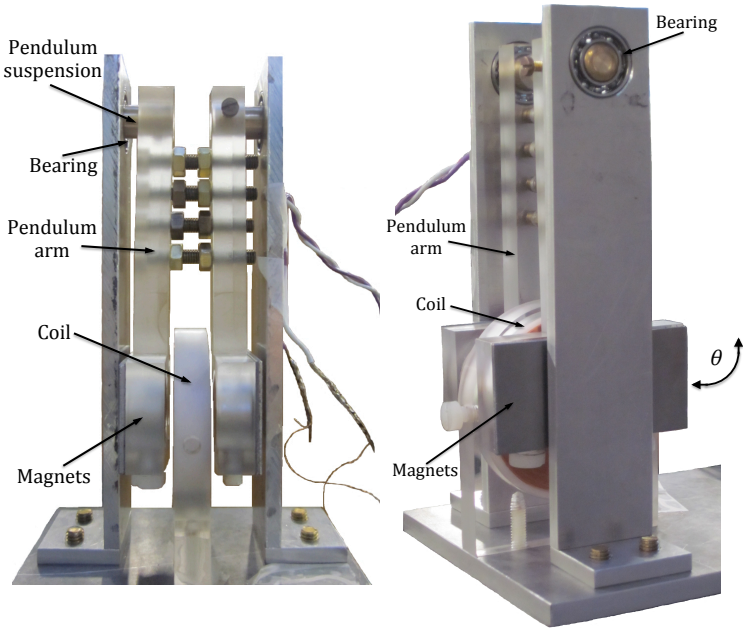

Figure 6: Electromagnetic pendulum harvester prototype: Swing.

and the magnets form the counter mass for the other end of the lever beam, which is then coupled to the electromagnetic transducer. The Swing and Corsair possess natural frequencies around 1.7 Hz and 4.5 Hz respectively .

3.3. Numerical analysis

Based on the numerical model previously established in [10] and the parameters listed in table 1, the initiation of parametric resonance was analysed for the two prototypes using ODE45 solver in MATLAB. A variation of the Strutt stability chart, plotting excitation frequency against input acceleration, for the Swing and Corsair prototypes are presented in figures 8 and 9.

Table 1: System parameters used to simulate the stability charts of the Swing and Corsair prototypes. Damping values are fitted to the experimental prototypes.

Parameter	**Swing**	**Corsair**	**Units**
Natural frequency	1.7	4.5	Hz
Pendulum length	86	12.2	mm
Lever length (pendulum side)	n/a	25	mm
Lever length (transducer side)	n/a	30	mm
Pendulum mass	0.205	0.097	kg
Lever counter mass	n/a	0.080	kg
Mechanical parasitic damping	84.4	18.8	$\mathrm{N{\cdot}s{\cdot}m^{-1}}$
Electrical transducer damping	291	295	$\mathrm{N{\cdot}s{\cdot}m^{-1}}$

It can be seen that the application of electrical damping, as the mechanical-to-

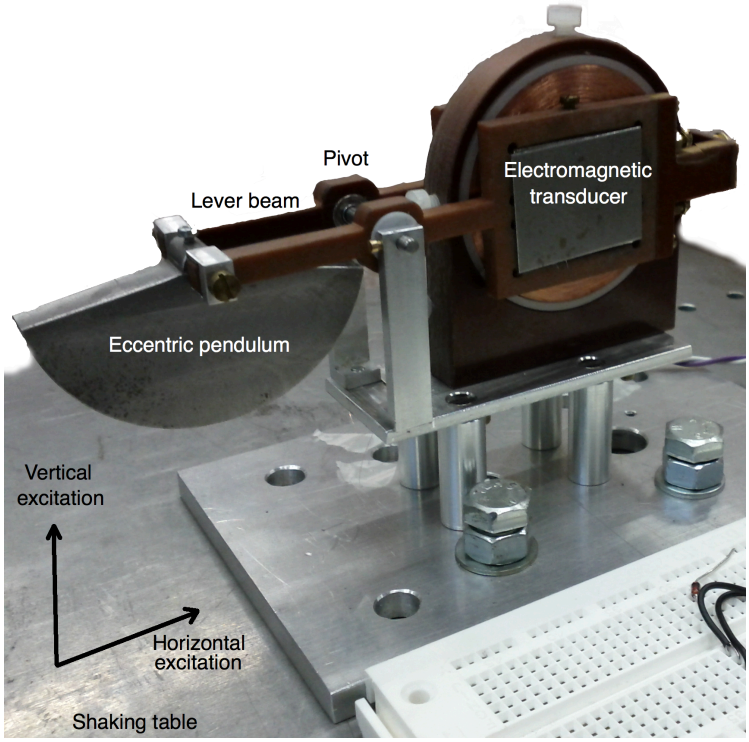

Figure 7: Electromagnetic pendulum-lever harvester prototype: Corsair.

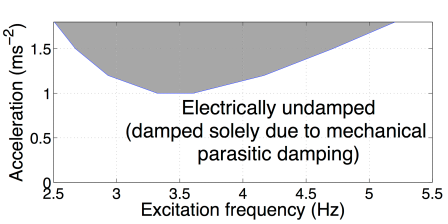

(a) Electrically undamped

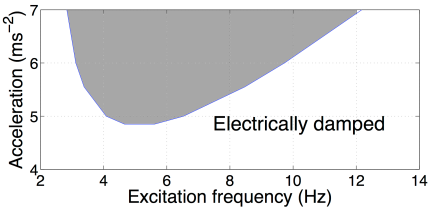

(b) Electrically damped - significantly higher initiation threshold amplitude

Figure 8: Simulated stability chart of the Swing prototype where the pendulum is electrically damped to complete the mechanical-to-electrical energy conversion. Shaded region represents the unbounded solutions of the Mathieu equation and the onset of parametric resonance. The addition of electrical damping pushed the initiation threshold from ~ 1 ms^{-2} to ~ 4.8 ms^{-2}.

electrical transducer is in operation, a noticeable increase in the initiation threshold of parametric resonance for the Swing prototype occurs. On the other hand, the presence of electrical damping has minimal effects on the Corsair prototype as the pendulum (the parametric resonator) is not directly subjected to the electrical damping of the transducer and is still allowed to freely build-up its oscillatory amplitude.

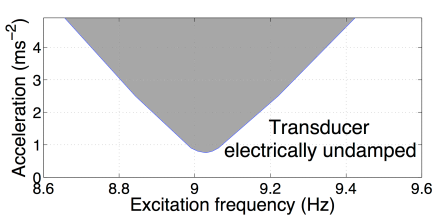

(a) Electrically undamped

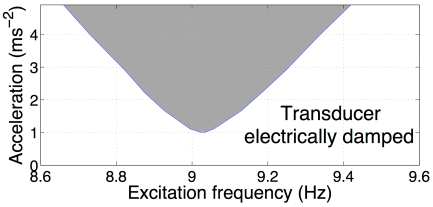

(b) Electrically damped - slightly higher initiation threshold amplitude

Figure 9: Simulated stability chart for the Corsair prototype where the pendulum is intrinsically electrically undamped and the lever beam is electrically damped as the transducer. Shaded region represents the unbounded solutions of the Mathieu equation and the onset of parametric resonance. The addition of electrical damping pushed the initiation threshold from ~ 0.76 ms^{-2} to ~ 1.0 ms^{-2}.

3.4. Power and threshold

Prototypes were subjected to direct (horizontal) and parametric (vertical) excitation from the shaker. Parametric resonant onset at 3.4 Hz (twice the natural frequency) for the Swing has been observed for an electrically undamped (open circuit) configuration when a minimum acceleration of approximately 1 ms^{-2} is attained. However, with the application of the resistive load ($\sim$17.6 kΩ), parametric resonance failed initiate within the scanned acceleration range limited by the physical constraint of the shaker (maximum displacement $\sim$10 mm, which translates to 4.56 ms^{-2} for 3.4 Hz).

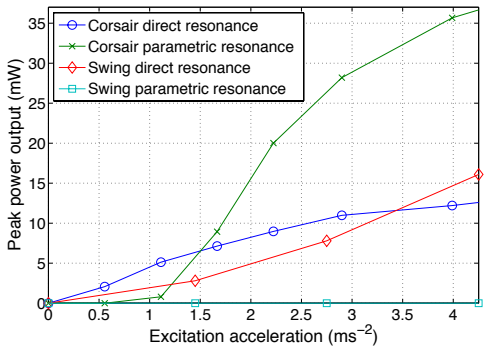

Figure 10: Power response per excitation acceleration levels for the electromagnetic Swing (pendulum) and Corsair (pendulum-lever) prototypes.

On the other hand, the onset of parametric resonance for the electrically damped Corsair was much more readily accessible at lower acceleration levels as shown in figure 10. The pendulum can freely build up its oscillatory amplitude with relatively less restriction, since it is not directly coupled to the electrical damping of the transducer and the damping term in equations 5 and 6 is lower for this prototype compared the Swing design.

The initiation threshold amplitude of the Corsair under matched optimal electrical load ($\sim$16.8 kΩ) was recorded at 1.11 ms^{-2} and the power performance of parametric resonance outraced direct resonance for accelerations in excess of approximately 1.5

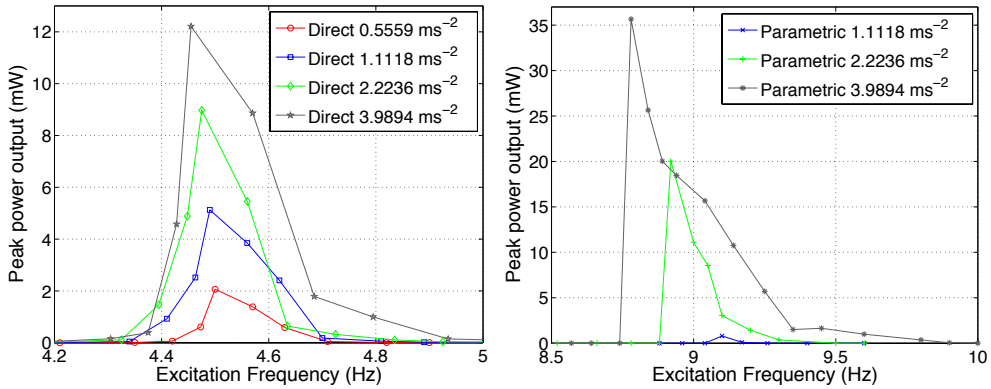

(a) Direct resonance (b) Parametric resonance

Figure 11: Power response of Corsair (f_n∼4.5 Hz) in the frequency domain.

ms^{-2}. Figure 11 presents the frequency characteristics of the Corsair. At an excitation of 3.99 ms^{-2}, 12.21 mW (half power band of 0.17 Hz) and 35.67 mW (half power band of 0.20 Hz) were recorded for the direct resonant and parametric resonant peaks.

As acceleration increases and pushing device operation deeper into the profitable region, the power performance gap of parametric resonance over its direct counterpart further widens. The onset of nonlinearities at high amplitudes help to mildly broaden the resonant peaks. No higher orders of parametric resonance were observed, potentially due to the fast narrowing nature of the frequency bandwidth of these higher orders. The same parametric amplification characteristics is theoretically predicted for the Swing prototype as well, but the onset of parametric resonance, when electrically damped by the transducer, is at a larger acceleration level than that attainable by the mechanical shaker employed at this frequency.

4. Route II: piezoelectric cantilever and initial spring configuration

4.1. Design

Unlike the design from the previous section, the parametric resonators here are directly subjected to electrical damping from a piezoelectric transducer. Figure 12a illustrates a simple cantilever whose oscillatory displacement in the x plane is electrically damped. Horizontal forcing along the same x plane corresponds to a direct excitation, while orthogonal driving force such as in the vertical direction can potentially act as the parametric excitation. In figure 12b, an orthogonal clamped-clamped beam is added to the structure prior to the anchor. This additional initial spring directly displaces along the same direction as the parametric excitation in the vertical axis. Therefore, the base vibration of parametric excitation along the vertical axis undergoes additive mechanical amplification before being fed into the vertically upright cantilever beam. Although the initial beam can lower the initiation threshold amplitude of parametric resonance [12], it also acts as an additional source of energy dissipation. The following sections investigates various design parameters in an attempt to optimise this threshold-aided cantilever-based parametric resonant harvester.

When the natural frequency of the initial spring is matched to two times that of

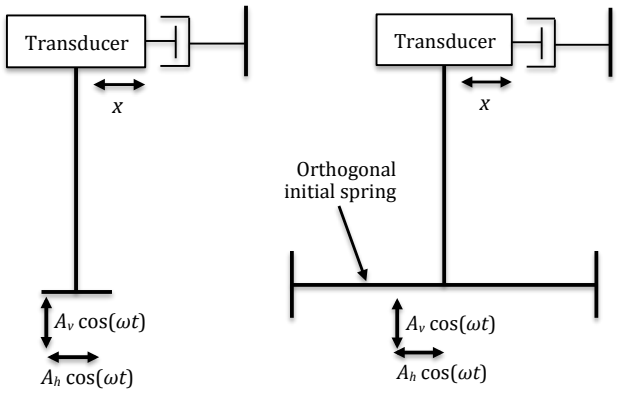

(a) Cantilever (b) Addition of initial spring

Figure 12: Design iteration with the addition of initial spring to amplify the base excitation fed into the parametric resonator (cantilever beam).

the cantilever beam in figure 12b, a direct resonant amplification of the parametric excitation can be achieved. This is known as auto-parametric resonance, where the energy build up from direct resonant input into an initial resonator in a multiple degree-of-freedom system is internally transferred to a secondary resonator as an internal parametric resonance [9].

Auto-parametric resonators possess the advantage of lower initiation threshold due to this resonant-based amplification for the parametric excitation. Alternatively, there is a frequency bandwidth advantage from tuning the natural frequencies away from this 2-to-1 frequency ratio and sacrificing the auto-parametric effect in order to exhibit multiple resonant peaks.

Cantilever beam driven by direct excitation in the direction of displacement x can be represented by equation 7.

$$\ddot{u} + 2c_1\dot{u} + c_2\dot{u}|\dot{u}| + \mu u^3 + \omega_0^2 u = \omega^2 X \cos(\omega t) \tag{7}$$

where, u and X are the dimensionless quantities of response displacement in the x axis and direct excitation displacement A_h normalised against beam length l, c_1 is the linear viscous damping parameter, c_2 is a quadratic damping representing the dominant higher order damping nonlinearity, μ is a parameter representing cubic geometric non-linearities, ω is the excitation frequency and ω_0 is the angular natural frequency. The parameters c_1, c_2 and μ are normalised parameters against effective mass. Parametric excitation applied in the orthogonal direction of the displacement is given by equation 8 [15, 19].

$$\ddot{u} + 2c_1\dot{u} + c_2\dot{u}|\dot{u}| + \mu u^3 + (\omega_0^2 - \omega^2 Y \cos(\omega t))u = 0 \tag{8}$$

where, Y is the parametric excitation displacement A_v normalised against l.

4.2. Apparatus

Figure 13 presents the piezoelectric cantilever-based harvester set up for both direct and parametric excitations. A single cantilever beam configuration and the addition of a clamped-clamped beam (single or double) as the initial spring is investigated

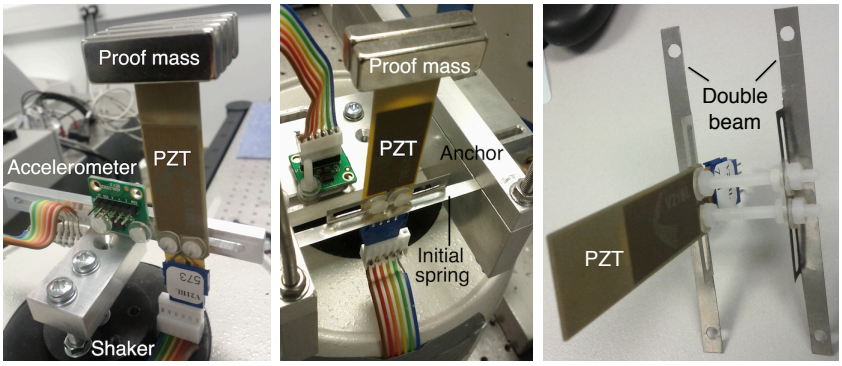

(a) Piezoelectric cantilever (b) With initial spring (c) With double beam

Figure 13: Cantilever-based harvester with initial spring to reduce the initiation threshold amplitude. Transverse forcing relates to direct excitation while acceleration along the long length of the beam can potentially represent parametric excitation.

Volture Systems V21BL from MIDE have been employed as the piezoelectric transducer. The transducer is made from a flexible laminate substrate, PZT with piezoelectric constant d_{31} of -190×10^{-12} C N^{-1} as well as an electromechanical coupling coefficient k_{31} of 0.36 and FR4 as the outer insulator coating. The electrodes sandwich the piezoelectric layer and primary strain is along the transverse direction of the beam, therefore, the primary operational mode utilises the d_{31} constant.

The beam is approximately 33.8 mm long and 14.2 mm wide of active piezoelectric bi-morph area near the supposedly clamped-end and a further ∼20.8 mm by ∼17.0 mm of non-piezoelectric beam area for the placement of proof mass. This design enables maximum strain near the clamped end of the beam, which is ideal for the piezoelectric transduction mechanism.

Multiple units of NdFeB magnets with dimensions of 30 mm by 10 mm by 5 mm and density of 7.4 gcm^{-3} were used as the proof mass. Initial beams were manufactured from stainless steel with various thickness iterations. A 3-axis accelerometer was used to control the acceleration fed into the vibratory system by a function generator controlled mechanical shaker fixed on a vibration isolation platform.

A number of system parameters and configurations were explored, which included:

- Effective mass (mainly relating to natural frequency and maximum strain)
  - Number of magnets attached
  - Positioning of the magnets along the beam length
  - Asymmetry induced from uneven number of magnets on either sides.
- Initial spring (mainly relating to initiation threshold of parametric resonance)
  - 3 thickness of beam: 101.6 μm, 152.4 μm and 203.2 μm
  - Active length of the clamped-clamped beam: 60 mm, 55 mm and 50 mm
  - Either single beam or double beam
  - Distance between the double beam

4.3. Power and threshold

4.3.1. Initial spring thickness Initial spring made from stainless steel had maximum active length of 60 mm and breadth of 5 mm with three thickness iterations of 101.6

μm, 152.4 μm and 203.2 μm. The configuration from figure 13b was setup with four pieces of symmetrically placed magnets near the free end of the beam.

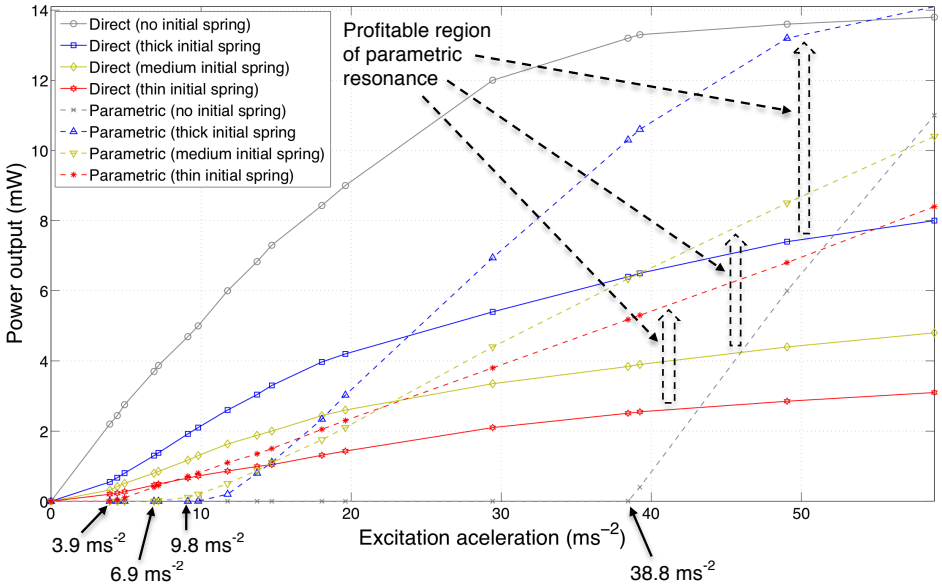

Figure 14: Power output per acceleration for piezoelectric cantilevers with and without the threshold-reducing initial spring structure.

It can be seen from figure 14 that the onset acceleration for parametric resonance is significantly reduced with the initial spring; from 38.8 ms^{-2} (no initial spring) to 9.8 ms^{-2} (thick initial spring), 6.9 ms^{-2} (medium initial spring) and 3.9 ms^{-2} (thin initial spring). However, this additional degree-of-freedom also acts as an energy dissipator. Stiffer the initial spring, more of the vibrational energy can propagate towards the subsidiary resonator and higher the quality factor. On the other hand, the earlier initiation of parametric resonance from more flexible initial springs maximises the profitable regions over direct resonance. Therefore, an optimal balance exist where this superior resonant phenomenon can be activated at relatively low acceleration while not sacrificing too much energy in the initial spring.

Direct resonant power output steadily increases with input acceleration until the approaching the physical limits of the piezoelectric transducer. The power slopes for both direct and parametric resonances flatten with thinner initial springs. Although the initial spring parametric curves demonstrated large profitable regions over direct counterparts, improvement over the sole cantilever structure was only observed for the thick initial spring iteration in excess of 56 ms^{-2}. Further widening of the profitable region was limited by the transducer limits employed here.

4.3.2. Strain compromise from the addition of initial spring While other mechanical-to-electrical transducers like electromagnetic and electrostatic rely primarily on displacement maximisation, piezoelectric focuses on strain maximisation. Therefore, the addition of the initial spring structure, despite the ability for the system to attain high displacement when parametric resonance is activated, compromises the

effective strain across the piezoelectric region on the main cantilever compared to a sole cantilever design as can be seen in figure 15.

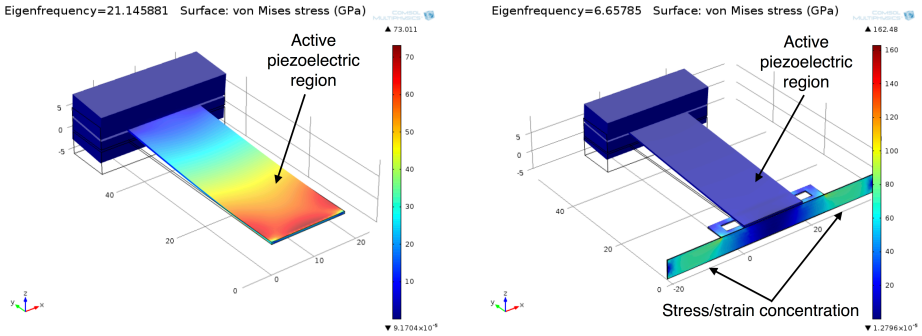

(a) Cantilever without initial spring, 1st bending mode eigen-frequency = 21.1 Hz

(b) Cantilever on an initial spring, 1st bending mode eigen-frequency = 6.66 Hz

Figure 15: Although initial spring structure helps to activate parametric resonance at lower excitation amplitudes, strain maximisation during deflection is compromised across the main cantilever beam, which is important for piezoelectric transducers. Stress is concentrated around the initial spring rather than the active piezoelectric region on the main cantilever.

Henceforth, the significant power advantage of parametric resonance over a comparable direct resonant system without the threshold-reducing designs, as observed for earlier parametric resonant harvesters for both electromagnetic (section 3) and electrostatic [13, 14] transducers, were not obvious for the piezoelectric system here.

4.3.3. Further stiffness variation The similar trend from figure 14 was observed where the stiffness of the initial spring was further tuned either by changing the active length or by varying the proof mass. While shorter beam corresponds to lower flexibility, larger proof mass yields the opposite result. The addition of a second parallel initial spring was aimed to provide additional stiffness variation. However, the double beam structure appears to worsen in both power output and initiation threshold amplitude from the increased damping and energy dissipation. Nonetheless, as the distance between the double beam widens, the experimental trend projects a decrease in initiation threshold amplitude.

4.3.4. Transient state The transient build-up time required for parametric resonance is almost always longer than direct resonance and is directly dependent on the acceleration amplitude relative to the initiation threshold amplitude. As acceleration increases beyond this threshold and move deeper into the instability region of the Strutt diagram, shorter time is required to reach the non-trivial steady-state solution.

4.3.5. Variation in T-shape The transverse mode of the cantilever beam here is along the narrow breadth of the clamped-clamped initial spring instead of the long length. The later configuration was investigated in an earlier study by the authors [11], but was difficult to achieve with the Volture piezoelectric beam employed here. As the cantilever beam vibrates along the more flexible plane of the clamped-clamped

beam, more energy is lost to displacement rather than strain on the piezoelectric and therefore compromises the quality factor.

4.3.6. Mass and frequency tuning All variable parameters investigated can tune the natural frequency of the system but the positioning and size of the proof mass are by far the most influential factors. Larger lumped mass and longer active length not only reduces the natural frequency but also yield greater power output per acceleration.

Another initiation criterion of parametric resonance is a non-zero initial displacement. Previous study has shown the advantage of the vertically upright mount over other mounting configurations [12, 11, 13], where comparisons can be drawn to an inverted pendulum. Asymmetrical proof mass further introduces an initial deflection, which helps to push the system into the instability region when the excitation is close to the initiation threshold.

4.3.7. Auto-parametric resonance The base excitation amplification exercised by the initial spring here is non-resonant. If the natural frequency of the clamped-clamped initial spring is tuned to twice that of the cantilever transverse mode, auto-parametric resonance can be achieved. It is a subset of parametric resonance where an externally driven direct resonator internally activates the parametric resonant response of a subsidiary resonator within the system. This would further minimise initiation threshold without sacrificing additional energy to an otherwise thinner initial spring. A recent publication by the authors on a different device has resulted in preliminary demonstration of this phenomenon [11]. However, the variability of the tuneable system parameters here did not accommodate for such natural frequency ratios.

4.4. Frequency domain characteristics

Figure 16 presents frequency domain voltage outputs (rectified across a matched optimal load) recorded from continuous frequency sweeps around the natural frequency. The natural frequency value agrees with the corresponding finite element model shown in figure 15b. Acceleration response is also shown in parallel due to the fixed displacement amplitude nature of the frequency sweep. Apart from the expected linear resonant peak of the 1st transverse mode of the cantilever beam, a second smaller resonant peak in the lateral plane (twisting) was also observed but the resultant strain on the piezoelectric layers was indirect and minuscule.

Figure 17 illustrates downwards frequency sweeps around twice the natural frequency. A slow 450 s sweep was undertaken to accommodate the long transient build-up required for parametric resonance. Once inside the instability region, frequency shifts within this region do not need to undergo this long build-up again.

Generally, significant portions of the nonlinear power response at frequency regions below than the natural frequency (right-hand side) do not show up during an upward sweep unless a significant displacement is already present, whereas downward sweeps reveal all the entire operational bandwidth. The onset of a steeper increase in response beyond a certain excitation amplitude was seen (figure 17b), which was absent for lower amplitudes (figure 17a). This indicates higher mechanical advantage and power output from a given drive acceleration, as the system moves deeper into the dominance of the instability region of the Mathieu equation.

At even higher amplitudes (figure 17c), a region of unsteady response can be seen prior to attaining the nonlinear resonant peak. This ‘knocking effect’ in the otherwise

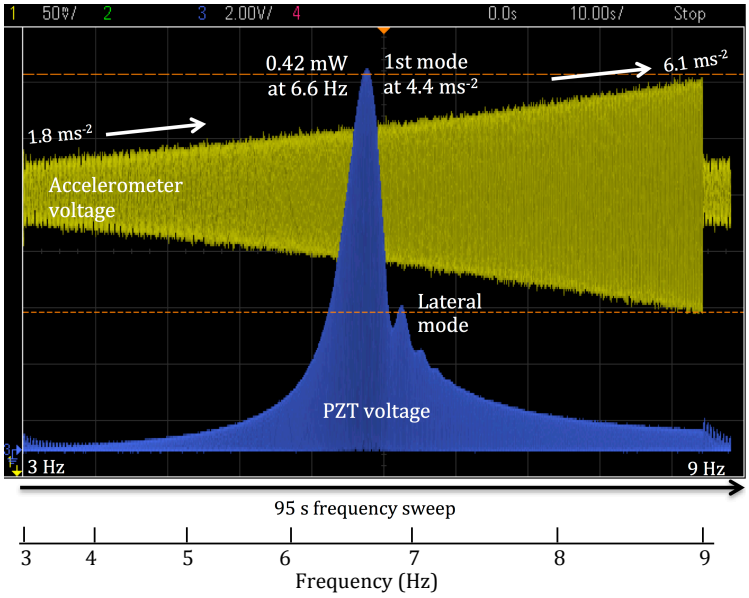

Figure 16: Oscilloscope voltage response from frequency sweep from 3 Hz to 9 Hz (around 1st mode of direct resonance ∼6.6 Hz) in the time domain.

steady-state is absent on either sides of this fluctuating frequency region. Figure 18 is a time domain scan at a fixed frequency within this unsteady band. A repetitive pattern of local minima and maxima can be observed. A potential explanation is that this band is within a nonlinear transition region for an amplitude dependent eigenfrequency shift. For a specific fixed excitation frequency, as the eigenfrequency begins to shift away, the response amplitude drops, which in turn returns the eigenfrequency before the next cycle. An alternative physical explanation is the possible modulated energy drain to another nonlinear coupled mode that becomes significant at specific amplitude and frequency conditions.

5. Conclusion

This work investigated prototype iterations of two distinct design routes in an attempt to passively minimise the initiation threshold amplitude required to access parametric resonance. This alternative resonant phenomenon can offer additional resonant regimes and potential power amplification over direct resonance. While one design route investigated an electrically undamped parametric resonator (pendulum) coupled to an electrically damped (electromagnetic) subsidiary mechanical amplifier (lever beam); the other approach involved an electrically undamped mechanical amplifier (clamped-clamped initial spring) coupled to a subsidiary electrically damped (piezoelectric) parametric resonator (cantilever beam). Up to an order of magnitude lower initiation threshold was experimentally observed for both designs. Ongoing and future work include auto-parametric resonant harvesters to lower initiation threshold without sacrificing significant energy dissipation as well as multifrequency operation from a coupled direct and parametric resonant system.

Acknowledgments

This work was supported by the Engineering and Physical Sciences Research Council (grant number EP/I019308/1). The authors would also like to express gratitude to Mr Gareth Ryder for helping to construct the electromagnetic harvester prototypes.

References

[1] S. Priya and D.J. Inman. *Energy Harvsting Technologies*. Springer US, New York, 2009.
[2] A.H. Nayfeh and D.T. Mook. *Nonlinear Oscillations*. Wiley-Interscience, New York, 1979.
[3] E.I. Butikov. Parametric resonance in a linear oscillator at square-wave modulation. *Eur. J. Phys.*, 26(1):157–174, 2005.
[4] D.W. Carr, S. Evoy, L. Sekaric, H.G. Craighead, and J.M. Parpia. Parametric amplification in a torsional microresonator. *Appl. Phys. Lett.*, 77(10):1545–1547, 2000.
[5] M.V. Requa and K.L. Turner. Electromechanically driven and sensed parametric resonance in silicon microcantilevers. *Appl. Phys. Lett.*, 88(26):263508 (3pp), 2006.
[6] M.J. Thompson and D.A. Horsely. Parametrically amplified mems magnetometer. In *Proc. Transducers 2009*, pages 1194–1197, Denvor, CO, 21-25 June 2009.
[7] M.F. Daqaq and D. Bode. Exploring the parametric amplification phenomenon for energy harvesting. *Proc. Inst. Mech. Eng. I J. Syst. Control Eng.*, 225(4):456–466, 2011.
[8] Nicholas Minorsky. *Nonlinear Oscillations*. Robert E. Krieger, New York, 1974.
[9] A. Tondl, T. Ruijgrok, F. Verhulst, and R. Nabergoj. *Autoparametric resonance in mechancial systems*. Cambridge University Press, Cambridge, UK, 2000.
[10] Y. Jia, J. Yan, K. Soga, and A.A. Seshia. A parametrically excited vibration energy harvester. *J. Intel. Mat. Syst. Str.*, DOI: 10.1177/1045389X13491637, 2013.
[11] Y. Jia and A.A. Seshia. Directly and parametrically excited bi-stable vibration energy harvester for broadband operation. In *Proc. Transducers 2013*, volume DOI: 10.1109/Transducers.2013.6626801, pages 454–457, Barcelona, Spain, 16-20 June 2013.
[12] Y. Jia, J. Yan, K. Soga, and A.A. Seshia. A mems parametrically excited vibration energy harvester. In *PowerMEMS*, pages 215–218, Atlanta, Georgia, 2-5 December 2012.
[13] Y. Jia, J. Yan, K. Soga, and A.A. Seshia. Parametrically excited mems vibration energy harvesters with design approaches to overcome initiation threshold amplitude. *J. Micromech. Microeng*, 23(11):10pp., 2013.
[14] Y. Jia, J. Yan, K. Soga, and A.A. Seshia. Multi-frequency operation of a mems vibration energy harvester by accessing five orders of parametric resonance. In *J. Phys. Conf. Ser.*, volume 476 of *1*, pages pp. 607–611, 2013.
[15] M.F. Daqaq, C. Stabler, Y. Qaroush, and T. Seuaciuc-Osorio. Investigation of power harvesting via parametric excitations. *J. Intel. Mat. Syst. Str.*, 20(5):545–557, 2009.
[16] L.A. Oropeza-Ramos and K.L. Turner. Parametric resonance amplification in a memgryoscope. In *Proceedings of IEEE Sens.*, page 4pp, Irvine, CA, 30 October - 3 November 2005.
[17] M. Sharma, E.H. Sarraf, and E. Cretu. Parametric amplification/damping in mems gyroscopes. In *IEEE MEMS*, pages 617–620, 17 March 2011.
[18] S.P. Beeby, R.N. Torah, M.J. Tudor, P. Glynne-Jones, T. O'Donnell, C.R. Saha, and S. Roy. A micro electromagnetic generator for vibration energy harvesting. *J. Micromech. Microeng*, 17(7):1257–1265, 2007.
[19] M.P. Cartmell. The equations of motion for a parametrically excited cantilever beam. *J. Sound Vib.*, 143(3):395–406, 1990.

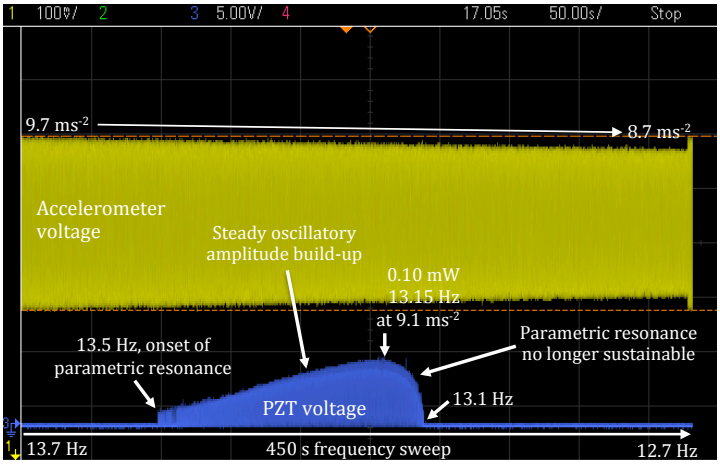

(a) Linear build-up

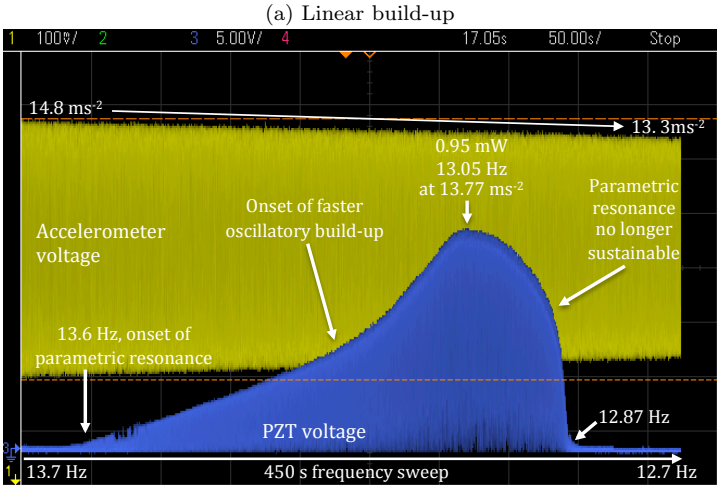

(b) Onset of steeper peak

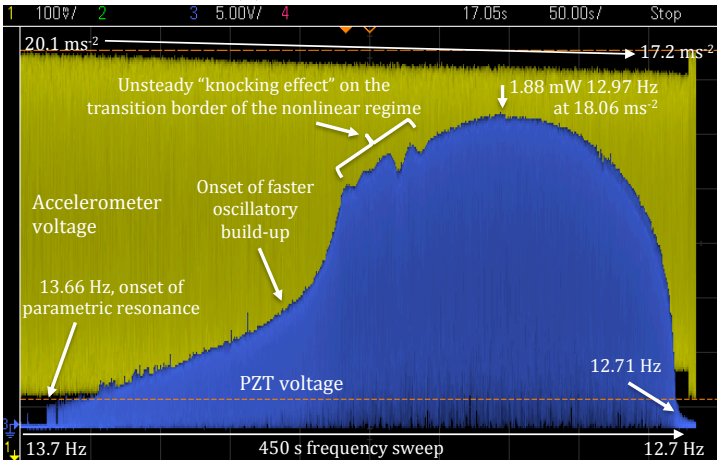

(c) Onset of unsteady state

Figure 17: Oscilloscope voltage response of frequency sweep from 13.7 Hz to 12.7 Hz (around principal (1st order) parametric resonance) in the time domain with varying acceleration levels.

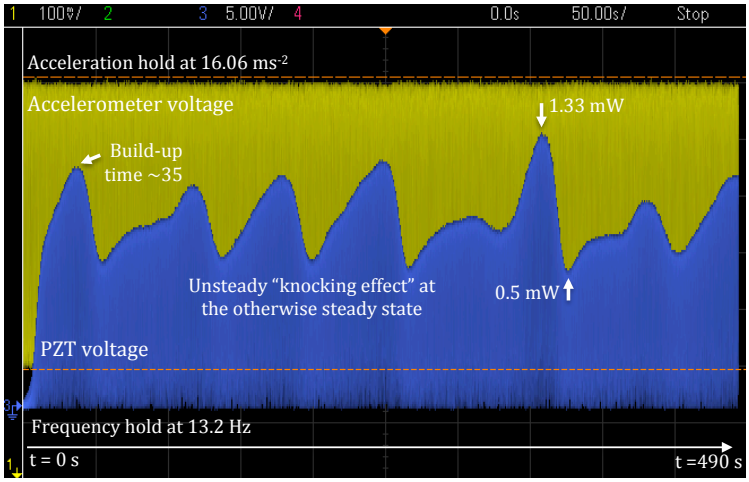

Figure 18: Unsteady state for certain transitional frequency regions of the parametric resonant response at high amplitudes.